Dalton Transactions

A Zr Metal-Organic Framework based on tetrakis(4-carboxyphenyl) silane and factors affecting the hydrothermal stability of Zr-MOFs

Journal:	*Dalton Transactions*
Manuscript ID:	DT-ART-01-2015-000421.R2
Article Type:	Paper
Date Submitted by the Author:	25-Mar-2015

Complete List of Authors:	Wang, Shufen; Nanjing Normal University, Department of Chemistry Wang, Jingjing; Nanjing Normal University, Department of Chemistry Cheng, Weiwei; Nanjing Normal University Taizhou College, School of Chemistry and Bioengineering Yang, Xiaowei; Nanjing Normal University, Department of Chemistry Zhang, Zaiyong; Nanjing Normal University, Department of Chemistry Xu, Yan; State Key Laboratory of Materials-oriented Chemical Engineering, College of Chemistry and Chemical Engineering Liu, Hongke; Nanjing Normal University, Jiangsu Collaborative Innovation Center of Biomedical Functional Materials, Jiangsu Key Laboratory of Biomedical Materials, College of Chemistry and Materials Science Wu, Yong; Nanjing Normal University, Chemistry Fang, Min; Nanjing Normal University, Department of Chemistry

Dalton Transactions

RSCPublishing

PAPER

A Zr Metal-Organic Framework based on tetrakis(4-carboxyphenyl) silane and factors affecting the hydrothermal stability of Zr-MOFs

Shufen Wang,[a] Jingjing Wang,[a] Weiwei Cheng,[b] Xiaowei Yang,[a] Zaiyong Zhang,[c] Yan Xu,[d] Hongke Liu,[c,e] Yong Wu,*[a] Min Fang*[a,e,f]

Cite this: DOI: 10.1039/xOxxOOOOOx

Received OOth January 2012, Accepted OOth January 2012

DOI: 10.1039/xOxxOOOOOx

www.rsc.org/dalton

A new (4,8)-connected Zr-MOF porous zirconium metal−organic framework (Zr-MOF) with flu topology, $Zr_6(\mu_3–O)_4(\mu_3–OH)_4(TCPS)_2(H_2O)_4(OH)_4$ (**1**, TCPS = (tetrakis(4-carboxyphenyl) silane) with a BET specific area of 1402 m^2g^{-1} has been constructed and fully characterized. **1** is stable in air and acid media but unstable in water and basic media, and thermally stable up to 200 °C. The new MOF is a wide band gap semiconductor with E_g = 3.95 eV. The excitation of **1** at 260 nm gives a ligand-based emission peak at 435 nm. After solvent exchange processes and activation at 200 °C, this MOF exhibits high storage capacities for H_2, CH_4 and CO_2. We summarized the hydrothermal stability data of Zr-MOFs, calculated the NBO (natural bond orbital) charges of the coordinating oxygen atoms of the corresponding carboxylate ligands and analyzed the influencing factors. Besides the known reasons of hydrothermal stabilities of Zr-MOFs, we demonstrated that NBO charges of coordinating atoms of the ligands can be used to explain the hydrothermal stability of Zr-MOFs.

Introduction

Metal–organic frameworks (MOFs) are a rapidly growing class of porous solid-state materials built up from inorganic nodes and organic linkers.[1] They have received widespread attention owing to their potential applications in gas storage and separation,[2] catalysis,[3] chemical sensor,[4-5] semiconductor,[6-7] and supercapacitor.[8-9] However, most of the porous MOFs (20000 known[1]) are moisture-sensitive,[35] which greatly limited their desired potential applications in various fields. Hence, the emerging area of interest has been constructing of porous MOFs with high thermal and chemical stability.

Recently, zirconium-based metal−organic frameworks (Zr-MOFs) have attracted great attention because of their exceptional stabilities compared to those of other common MOFs.[10-15] The high affinity of zirconium towards oxygen linkers leads to resistance towards most chemicals and high thermal stability. However, it is difficult to obtain single crystals of zirconium carboxylate MOFs probably due to the fast formation of strong Zr-O bonds. Despite of huge efforts to synthesizing Zr-MOFs, only 34 Zr-MOF structures† have been made and 21 of them were obtained based on single crystal X-ray diffraction data.

Tetratopic carboxylate linkers with tetrahedral geometry appear to be very intriguing building units in MOF constructions and have gained an increasing amount of attention in recent years,[16-29] The tetrahedral linker has a full Td symmetry,[30] which is, by far, the highest symmetry in a linker that can be achieved through organic synthesis. In addition, the tetrahedral linker is an inherently three-dimensional, fully extended strut. However, only two Zr-MOFs based on tetrahedral ligands were reported.[16-17] Both of them are flu topology (CaF_2), which represents a network that combines 4-connected tetrahedral linkers and 8-connected cubical secondary building units (SBUs) in a 2:1 ratio with no self-interpenetration,[17] resulting in high porosity. However, the investigated properties of both were not all-inclusive, especially the hydrothermal stability.

Here, we reported another novel Zr-MOF with flu topology, $Zr_6(\mu_3–O)_4(\mu_3–OH)_4(TCPS)_2(H_2O)_4(OH)_4$ (**1**) based on the tetrahedral carboxylates linker, tetrakis(4-carboxyphenyl) silane (TCPS)，which is the first Zr-MOF based on a silane ligand. Although, the Zr-MOF based on the tetrakis(4-carboxyphenyl) methane (TCPM)) (MOF-841) have been reported by the Yaghi et al, only the water adsorption of MOF-841 was investigated, which is one of the top performers among the 11 Zr-MOFs and other 11 porous solids.[16] Tetrahedral silicon centers are in general more synthetically accessible than their carbon equivalents and are thus promising candidates for a series of new connecting units with easily modifiable structural and chemical properties.[31] **1** and MOF-841 have the same topology. By replacing the central carbon with silicon, we found 4 $HCOO^-$ ligands to the Zr_6 core (the common SBU in Zr-MOFs) in the MOF-841 have been replaced with 4 OH^- ligands.

After solvent exchange processes and activation at 200 °C, this MOF exhibits high storage capacities for H_2, CH_4 and CO_2. When excited by light of 260 nm wave length, **1** has a ligand-based emission at 435 nm. **1** absorbs ultraviolet light, and the corresponding well-defined optical absorption associates a band gap (E_g) of 3.95 eV. Thus, **1** is a wide gap semiconductor.[26] This material can be used safely in air and acidic solution and stable up to

200 °C and decomposes at 250 °C. We found **1** lost crystallinity after soaked in water and basic solution for 12 h. We summarized the hydrothermal stability data of Zr-MOFs, calculated the NBO (nature bond orbital) charges of the coordinating oxygen atoms of the corresponding carboxylate ligands and analyzed the influencing factors. Besides the known reasons of hydrothermal stabilities of Zr-MOFs,[32-33] we demonstrated that NBO (nature bond orbital) charges of coordinating atoms of the ligands can be used to explain the hydrothermal stability of Zr-MOFs.

Experimental

Materials and general methods

Reagents were obtained from commercial sources and used without further purification, and the ligand TCPS, was prepared according to the literature.[34] Infrared spectra (FTIR) were recorded in the range 400–4000 cm^{-1} on a Bruker Vector 22 infrared spectrometer. Elemental analyses for C and H were performed on Vario EL III elemental analyzer of Nanjing Normal University. TG-DTA was carried out using the SDT 2980 thermal analyzer under the N_2 flow of 15 mL/min over the temperature range from 25 °C to 600 °C at a heating rate of 5°C min^{-1}. Powder X-ray diffraction (PXRD) patterns were performed on a Bruker D8 Advance instrument using Cu Kαradiation (λ = 1.54056 Å) with a scan speed of 0.1 s per degree at room temperature. Surface area and pore characteristics measurements were measured by Micromeritics ASAP 2050 Extended Pressure Adsorption Analyzer using N_2. And H_2 adsorption isotherms at 77 K up to 10 bar were also measured on the ASAP 2050 instrument. Before analysis, the pre-treated MOF samples were degassed at 200 °C under vacuum for 10 h. UV-Vis diffuse reflectance spectral measurements were carried out using Varian Cary 5000 UV -Vis-NIR. The fluorescence spectra were recorded by a FM-4P-TCSPC Transient State Fluorescence Spectrometer.

Synthesis $Zr_6O_4(OH)_4(TCPS)_2(OH)_4(H_2O)_4$

TCPS（6.40 mg, 0.0125mmol), and $ZrOCl{\cdot}8H_2O$ (16.10 mg, 0.0500 mmol) were ultrasonically dissolved in a solvent mixture of DMF (2 mL) and formic (1.2 mL) acid. The mixture was then heated at 130°C for 2 days. After cooling to room temperature, colorless distorted-octahedron-shaped crystals were collected by filtration, and washed with DMF and dried in a 40 °C oven for 10 h (Yield: 11 mg, 58% based on H_4TCPS). The products are denoted as "as-synthesized". Its purity was checked by PXRD. FTIR (KBr, ν/cm^{-1}): 3410 (m)，1668 (s)，1603 (m), 1534 (m), 1414 (m)， 1104 (w)，775 (m), 726 (m)，653 (m)，472 (m). The sample was activated at 200°C for 12 h before the elemental analysis. Elemental analysis for $Zr_6O_4OH_4(COO)_8(OH)_4(H_2O)_4$, calcd (%): C 35.21, H 2.51 Found (%): C 35.24, H 2.66.

As-synthesized **1** was put in 10 mL of anhydrous DMF with a few drops of 2 M HCl for 12 h, and then immersed in 10 mL of anhydrous acetone for 3x12 h, during which the acetone was decanted and replaced with fresh acetone every 12 h. After the removal of acetone by decanting, the sample was dried in a 40 °C oven for 10 h, which was denoted as "solvent exchanged" sample.

X-ray crystallography

Suitable crystals of compound **1** were selected for single crystal X-ray diffraction. The data were collected at 296 K on a Bruker Smart CCD diffractometer with graphite-monochromatic Kα radiation (λ=0.71073 Å) from an enhanced optic X-ray tube. Raw data for the structure were obtained using SAINT, and absorption correction was applied using SADABS programs. The structure was solved by the direct method and refined by full-matrix least-squares on F^2, using the SHELXS-97 and SHELXL-97 program. A summary of the crystallographic data, data collection, and refinement parameters for complex is provided in Table S1 (SI).

Results and discussion

Description of the structure

Single crystal X-ray diffraction reveals that the compound crystallizes in the tetragonal space group I4/m, which also belongs to 4, 8-connected 3D network with flu topology (Fig. 1). Two other Zr-MOFs based on tetrahedral linkers have the same topology.[16-17] There are two kinds of lengths of the bonds between Zr and terminal oxygens which is 2.185(3) Å and 2.212(3) Å. We assigned these oxygens to be four OH^- and four H_2O, respectively. Zr−H_2O bond in PCN-222 is reported as 2.21 Å.[35] Correspondingly, there also exists two different Zr-O distances (2.135 Å and 2.179 Å), we assigned the these oxygens to be μ_3-O^{2-} and μ_3-OH^-, respectively. Therefore the cluster formula in compound **1** is assigned to be $Zr_6(\mu_3{-}O)_4(\mu_3{-}OH)_4(COO)_8(OH)_4(H_2O)_4$ (Fig. 1(b)) which is different from the $Zr_6(\mu_3{-}O)_4(\mu_3{-}OH)_4(COO)_8(HCOO)_4(H_2O)_2$ of MOF841, where the 4 $HCOO^-$ ligands (MOF-841) have been replaced with 4 terminal OH^- ligands (**1**). The structure is constructed by octahedron cages with diameters of 13.3 Å as shown in Fig.1 (d)，which is larger than the 11.6 Å of those in MOF-841. Channels with a window size of 10.2 Å × 7.98 Å (atom-to-atom distance after being deducted the van der Waals radii of the related atoms) were observed when viewed along the *a* direction. The total solvent accessible volume of compound **1** is 62.6% determined by PLATON which is also larger than that of MOF-841 (45.4%).[16]

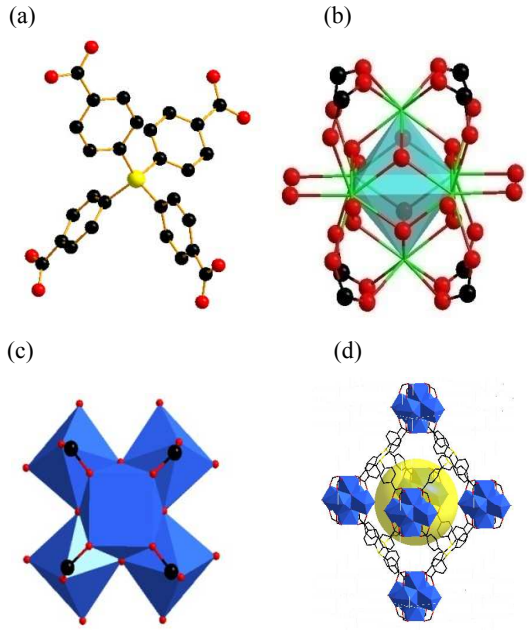

e)

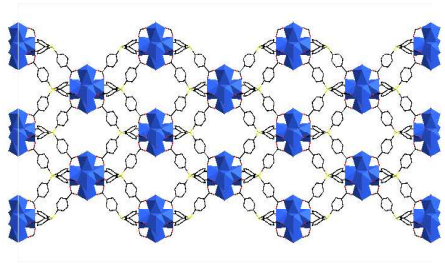

Fig. 1 (a) The structure of TCPS ; (b) $Zr_6O_4(OH)_4(COO)_8(OH)_4(H_2O)_4$ SBU; (c) The polyhedron of $Zr_6O_4(OH)_4(COO)_8(OH)_4(H_2O)_4$ cluster; (d) The octahedron cavity; (e) The 3D framework viewed from a axis;. (Atom color scheme: C, black; O, red; Zr, green; Si, yellow; Yellow ball represents the space in the framework).

Adsorption properties

The permanent porosity of compound **1** has been confirmed with the as-synthesized sample by nitrogen sorption experiments at 77 K (Fig. 2(i)). The N_2 uptakes of the as-synthesized sample is 380 cm^3 (STP)/g and the Brunauer−Emmett−Teller (BET) specific surface area is 1039 m^2g^{-1} and the Langmuir surface area is 1512 m^2g^{-1} with a pore volume of 0.60 cm^3g^{-1}. The H_2 uptakes is 1.26 wt% under 1 bar and 77 K, smaller than the 1.8 wt% for PCN-225, which has a BET surface area of 1902 m^2g^{-1}, nearly twice of **1**.[35] And under 10 bar and 77 K, the H_2 storage could reach up to 2.3 wt% and not to saturation, comparable to the 2.2 wt% of UiO-66 (The Langmuir surface area is 1281 m^2g^{-1}) [36] under the same condition (Fig. S1 in supporting information). To fully activate **1**, we employed the solvent exchange method to replace the high boiling point solvents and other compounds involved in the as-synthesized sample, using acetone as the exchanging solvent. The N_2 uptakes of the "solvent exchanged" sample is 450 cm^3g^{-1} (STP) and the Brunauer−Emmett−Teller (BET) specific area is 1402 m^2g^{-1} and the corresponding Langmuir surface area is 1874 m^2g^{-1} with a pore volume of 0.69 cm^3g^{-1}. The presence of a small hysteresis step during desorption of N_2 is in agreement with the existence of mesopores. The BJH surface area and the pore volume of these mesopores are 220 m^2/g and 0.13 cm^3g^{-1}, respectively. The H_2 storage capacity of the solvent exchanged sample is very similar to that of the as-synthesized sample, reaching the maximum 2.3 wt% at 6.0 bar and 77 K, however decreases a little to 2.1 wt% at 10 bar (Fig. 2(ii)).

(i)

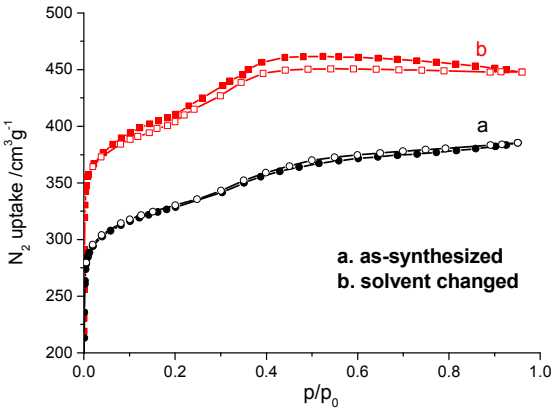

(ii)

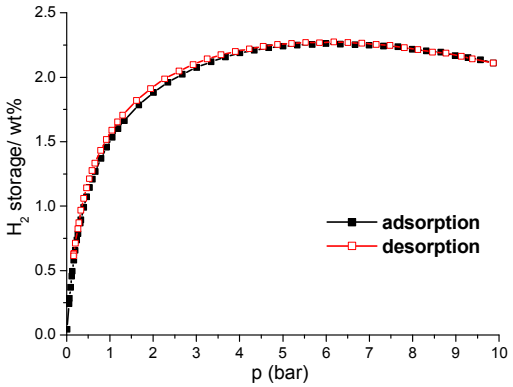

(iii)

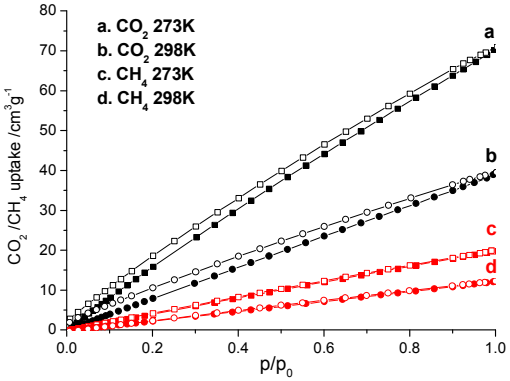

(iV)

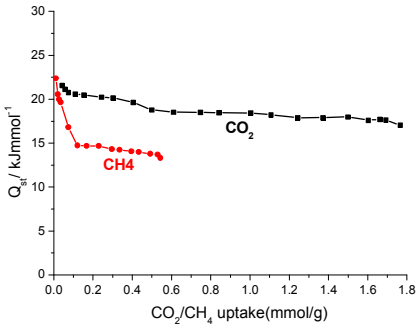

Fig. 2 Adsorption (closed symbol)/desorption (open symbol) isotherms (i) N_2 at 77 K of the solvent exchanged sample and as-synthesized sample; (ii) H_2 at 77 K of the solvent exchanged sample; (iii) CH_4/CO_2 at 293 K and 298 K of the solvent exchanged sample; (iv) the corresponding heats of CH_4/CO_2 adsorption of the solvent exchanged sample.

1 has high CO_2 and CH_4 uptake capacities (Fig. 2(iii)). The CO_2 and CH_4 uptakes of the solvent exchanged sample at 298 K and 1 bar are 39.5 cm^3 (STP)/g (1.8 mmol/g, 7.7 wt%) and 12.2 cm^3 (STP)/g (0.54 mmol/g, 0.9 wt%), respectively; which increases to 71.1 cm^3(STP)/g (3.2 mmol/g, 13.9 wt%) and 19.9 cm^3 (STP)/g (0.89 mmol/g, 1.4 wt%) when the temperature decreases to 273 K. These uptakes are higher than that of UiO-66 (Langmuir Surface area: 1066 m^2/g, 64.51 cm^3/g CO_2 at 273 K and 1 bar,[37] 6.72 cm^3/g CH_4 at 303 K and 1 bar.[38] UiO(bpdc) was recently reported as a material has high CO_2 and CH_4 uptakes.[39] The CO_2 (CH_4) uptakes of **1** are similar to that of UiO(bpdc),[39] which has a much larger BET surface area (2646 m^2/g) and absorbs 8.0 (1.0) wt% CO_2 (CH_4) and 13.0 (1.4) wt% at 1 bar and 293 K and 273 K, respectively.[39] The isosteric adsorption enthalpy (Q_{st}) of CO_2 of **1** lies in the range of 17.1–21.7 (Fig. 2(iv)), which is slightly lower than that of UiO(bpdc) (18.5–24.0), suggesting the moderate interaction strength of CO_2 with the framework.[40] The isosteric adsorption enthalpy (Q_{st}) of CH_4 of **1** lies in the range of 13.3-22.5 (Fig. 2(iv)) kJ mol^{-1}, which is greater than that of UiO(bpdc) (12.6–15 kJ mol^{-1}) and high among other MOF materials.[41] These studies indicate that **1** could be a very good material for CO_2 and CH_4 storage.

Hydrothermal stability

Thermogravimetric (TG) analysis of **1** showed three steps of weight loss prior to the formation of final ZrO_2 and SiO_2 products (Fig. 3). Based upon the calculated composition, 36.8% weight loss before 250 °C is due to DMF, formic acid and water within the pores or on the surface of the material. And the second step loss (4.8%) in the range of 250 to 300 °C is the coordinated water molecules and 4 additional waters formed by the 4 terminal OH^- and H in the μ_3-OHs in $Zr_6(\mu_3\text{–}O)_4(\mu_3\text{–}OH)_4$, consistent with the theoretical calculated value (4.77%). The final thermal decomposition begins at 450 °C, leaved 29.2% (ZrO_2 and SiO_2), which is also close to the theoretical value (28.0%). The powder XRD results (Fig. 3) showed that the framework began to lose crystallinity at 250 °C when the loss of water molecules happened. After being heated at 280 °C for 3 h, the BET surface area of **1** dropped to 75.9 m^2g^{-1}.

(i)

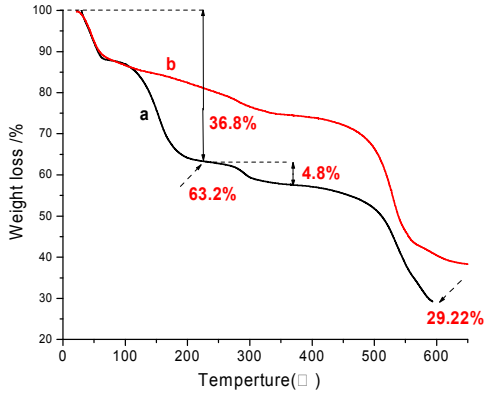

(ii)

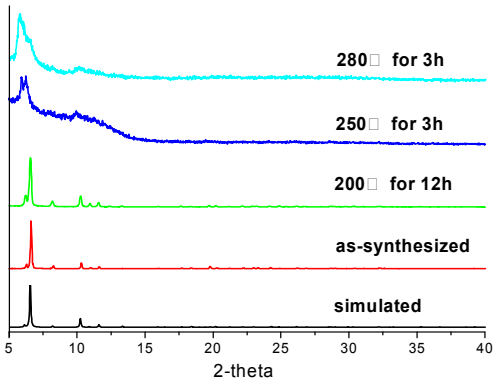

Fig. 3 (i) Thermogravimetric analysis of as-synthesized (a) and exchanged (b) **1**; (ii) The powder XRD patterns for simulated and as-synthesized **1** and as-synthesized **1** heated at different temperatures.

1 can be stable in acidic condition for 1 d and in air for 14 d as shown in Fig. 4. It can't retain crystallinity after soaked in the water for 12 h and unstable in basic conditions. For MOF-841, it could retain capacity of water adsorption after five adsorption/desorption cycles, and could be easily regenerated at room temperature. And Zhou et al. reported PCN-521 can be stable in air for 24 h. Their stability in water was not reported.[17]

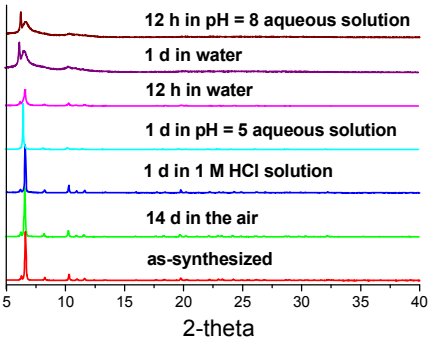

Fig. 4. The powder XRD pattern for simulated and as-synthesized **1** and as-synthesized **1** soaked in different water solutions.

Fluorescence property

We investigated the fluorescent property of **1.** Very few studies about the fluorescent property of Zr-MOFs were reported.[35, 42-43] The fluorescence emission of TCPS ligand at 435 nm (λ = 260 nm) (Fig. 5). The excitation of **1** at 260 nm also gives an emission peak at 435 nm but much narrower band, which means that the fluorescence emission is ligand based and coordination with Zr^{4+} has resulted stronger rigidity, leading to a narrower band.

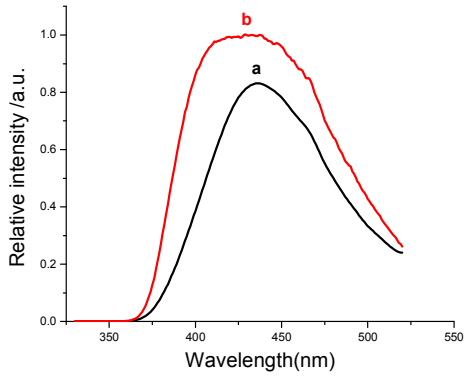

Fig. 5 Solid state photoluminescent spectra of **1** (a) and TCPS (b) The excitation wavelength is 260 nm.

UV-Vis diffuse reflectance spectrum and band gap of 1

Fig. 6 shows the UV-vis diffuse reflectance spectra of **1** and TCPS, and the characteristic absorption peaks of **1** was 283 nm which was close to 289 nm of TCPS. These absorptions were attributed to the π→π* transitions of the aromatic rings. The band gap of **1** and TCPS were determined based on the spectra. The band gap E_g was defined as the intersection point between the energy axis and the line extrapolated from the linear portion of the adsorption edge in a plot of the Kubelka–Munk function F versus energy E (the inset of Fig. 6). The Kubelka–Munk function, $F = (1-R)^2/2R$, was extracted from the recorded diffuse reflectance data, where R is the reflectance of an infinitely thick layer at any given wavelength.[44] The band gap (E_g) of **1** was found to be 3.95 eV, which is similar to that of the hydroxylated UiO-66 (4.07). The coordination to Zr^{4+} slightly increases the band gap of the ligand (from 3.85 to 3.95 eV). Similar to UiO-66, in which the organic linker causes a decrease of the band gap of ZrO_2 band gap (from 5.19 to 4.07), the organic linker reduces the bandgap of ZrO_2 to 3.95 eV; while for MOF-5, the organic linkers lead to an increase of E_g of the band gap of ZnO (from 3.4 eV to 5.0 eV).[45]

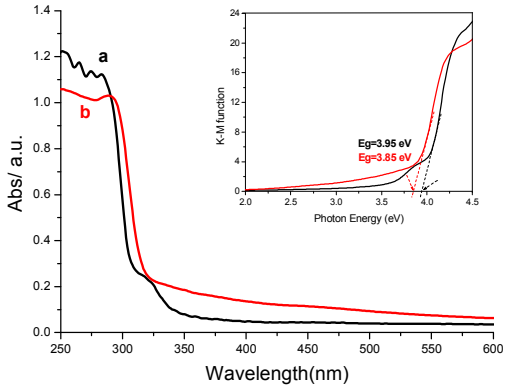

Fig. 6 Diffuse reflectance UV-vis spectra of **1** (a) and the linker TCPS (b); Inset: K-M function vs. energy (eV) of **1** (black) and TCPS (red).

The factors affecting the hydrothermal stability of Zr-MOFs

We summarized the hydrothermal stability data of Zr-MOFs in Table 1 and calculated the NBO charges of the coordinating oxygen atoms of the corresponding carboxylate ligands (shown in Scheme 1) using the reported method.[46] We have shown previously that the NBO charges of the coordinating atoms of the ligands can reflect the relative coordination abilities of the ligands to metal ions and the strength of the resulting M–L bonds. [46]

Many data in Table 1 did not reach the chemical stability limits of the investigated MOFs. A plateau in TG only means a new stable weight was reached. Therefore, whether it is still the same framework needs to be verified by PXRD. This is demonstrated by No. 12, 26 of Table 1 and the stability study of **1** (No. 43). There is a plateau at the temperature range of 300 - 400 °C in the TG of **1**, however, PXRD study shows it decomposes at 250 °C when losing the H_2O molecules from the structure. In addition, a sample should be reheated for a few hours and its stability is then checked by PXRD and this work is repeated until its decomposition temperature is found out. However, these works are seldom done in the literature as shown in Table 1.

According to variable PXRD results, the most thermally stable Zr-MOFs (No. 31, MIL-140C) can reach to up 500 °C, followed by UiOs (e.g. UIO-66, UIO-67) (~450 °C).[14] According to TG and XRD studies given in Table 1, 18 of them (50 in total) decompose at 400-500, 17 decompose at 300-390, 8 at 260-290, 5 at 200-250, 1 at 150 °C. Heating under vacuum could further reduce the decomposition temperature as shown by the case of Zr-BTC-formic (No. 39).[43] As reported by others, the initial bond breaking of Zr-MOFs could be Zr-O bond and C-C bond between the benzene ring and the carboxylate carbon,[11, 47] suggesting both C-C bond strength and Zr-O strength have effect on the thermal stability of Zr-MOFs.

Data in Table 1 indicate that Zr-MOFs are usually stable in acidic solutions, less stable in water and unstable in basic media. We calculated the NBO charges of O atoms of OH^- (-1.403) and H_2O (-0.997), which are significantly larger than the NBO charges of the O atoms of carboxylate ligands (-0.74 - -0.815). The NBO charges suggest that OH^- could form a stronger bond with Zr^{4+} than a carboxylate O atom, consistent with the fact that most of Zr-MOFs are usually unstable in basic media. In acidic solution, H_3O^+ cannot attack Zr-O bond effectively and also suppress the concentration of

OH^- in water. Therefore, Zr-MOFs are usually stable in acidic media. But in concentrated acid, the Zr-O could be protonated, leading to the weakening of the Zr-O bond (No. 22). Zhou et al. added specific amount of acid in the activation process of the Zr-MOFs to prevent structure decomposition in the long solvent-exchanging processes.[15] We found the higher NBO charges of the coordinated O atoms of the ligands, the higher water and chemical stability of the Zr-MOFs. For example, the NBO charges of L32 are high, leading to products which can be stable even in basic conditions for 24 h; UiO-66-F (No. 5) is more stable than UiO-66-F_2 (15); MIL-140A, B, C, D (No. 3, 24, 27 and 31) are isoreticular, and MIL-140D are found to be the least stable as indicated by the PXRD result, consisting with the smallest NBO charge of its ligand. The NBO calculation and the stability data in Table 1 suggest that Zr-MOFs should be stable in water (> 12 h) if the NBO charge of the O of the carboxylate ligands is greater than -0.756.

UiO-67 was reported as water unstable.[32] Farha et al.[33] demonstrated by PXRD and N_2 adsorption data that some Zr-MOFs, for example UiO-67 and NU-1000, are stable towards linker hydrolysis in H_2O, but collapse during the activation process when removing H_2O at elevated temperatures due to capillary forces. Importantly, they demonstrated that this framework collapse can be overcome by utilizing solvent-exchange with solvents having weak interactions with the framework such as acetone. Capillary forces are greatest when solvent surface tension is high and when solvent molecules adhere well to MOF cavities or channels (e.g., via strong hydrogen bonding). Processes such as solvent-exchange,[48] supercritical CO_2 ($scCO_2$) activation,[49] and freeze-drying have all been employed to help avoid channel collapse in MOFs.[50]

Based on the data in Table 1, we found that most Zr-MOFs can be stable in water for 12 h. The NBO charges of the ligands of those which were reported as water unstable usually have similar NBO charges to those of the stable ones, suggesting the Zr-O bonds of the seemly unstable Zr-MOFs are still as strong as those of water-stable ones. We therefore deduce that those unstable ones are very likely like UiO-67, stable in water. However, they decompose when removing water at elevated temperature due to capillary forces and were thought as water unstable. If they are exchanged with solvents like acetone, the frameworks would not have collapsed after activation. The water unstable ones in Table 1 usually have larger pores, suggesting capillary forces might be significant in these large pore structures. This is reasonable since more water could enter into a framework of large pores, which could results in stronger interactions between water and the framework. No. 32-35 and No. 45-48 Zr-MOFs have large pores, however, are reported as water stable since CH_2Cl_2 and acetone were used to exchange the original solvents in the pores of Zr-MOFs before activation. These work suggests these solvents could reduce the capillary forces. UiO-66-F and UiO-66-F_2 are unstable towards water and acetic acid, which could be due to the strong hydrogen bonding formed between F and H_2O molecules in the pores, leading to stronger capillary forces. Thus, capillary force is an important factor to affect both thermal and water stability of Zr-MOFs which calls for a proper activation procedure to be adopted to avoid this effect.

Peter Behrens et al. found the material which was activated by Soxhlet extraction with ethanol resulted in a material having the thermal stability up to 400 °C in contrast to the 280 °C of the synthesized sample (made in DMF, trace H_2O and benzoic acid). The reason for this could be that not all of the guest molecules were removed from Zr–abdc (as-synt.) by the standard washing procedure with DMF and ethanol. These remaining guests could then destroy the framework as they leave the material at 280 °C.[51] This is also the situation found by Peter Behrens et al. (No. 2)[52] Benzoic acid can be trapped in UiO-66 and cause partial decomposition at 300 °C. These examples indicate that synthetic methods and the activation procedures could affect the thermal stability of Zr-MOFs. The Soxhlet extraction method seems to be a good solvent exchange method and have not be widely applied.

Steric effect can also be an important factor. The substituent groups of the ligand can block guest molecules from easily accessing the carboxylate groups and subsequently breaking Zr–O bonds. The bigger steric effect of L28 compared to L27 and L30 compared to L29 results in the fact that PCN-57 (No. 33) is more stable than PCN-56 (No. 32), and PCN-59 (No. 35) more water stable than PCN-58 (No. 34). This effect is also recognized by others.[32] Jared B. DeCoste et al.[32, 53] proposed that the decreased stability of the double ring structures can be attributed to steric effects. The single ring Zr-MOFs have much narrower pores than the double ring Zr–MOFs not allowing access to the metal–carboxylate sites as well as prohibiting the organized clustering of solvent molecules to occur readily. Kusgens et al. suggested that hydrolysis of metal–carboxylate bonds in MOFs is driven by the ability of multiple water molecules to access and cluster around the metal–carboxylate sites.[53]

Hong-Cai Zhou et al.[13] explained the high hydrothermal stability of Zr-MOFs based on metalloporphyrins, proposing the introduction of OH groups improves the hardness of the Zr_6 core, which strengthens the bonding between the bridging ligands and the Zr_6 units, consisting with the experimental facts in Table 1. When using the same ligand, the stability was found to increase in the following order: 6-connected Zr_6 core (No. 47) > 8-connected Zr_6 core (No. 48) > 12-connected Zr_6 core (No. 49) ; 8-connected Zr_6 core (No. 20-21) > 12-connected Zr_6 core (No. 22). The importance of this factor needs to be further investigated.

Conclusions

In summary, a novel (4,8)-connected Zr-MOF (**1**) with flu topology based on the tetrahedral ligand (tetrakis(4-carboxyphenyl) silane has been synthesized and characterized. **1** possessed large octahedral cages with diameters of 13.3 Å, 62.6% solvent accessible volume (PLATON) and a BET surface area of 1402 m^2g^{-1}. **1** possesses high uptake capacity for H_2, CO_2 and CH_4. The exceptional stability and excellent adsorption capacities make this MOF a very promising material for CO_2 capture and energy gas storage.

The new MOF is a wide band gap semiconductor (E_g = 3.95eV). The excitation of **1** at 260 nm gives a ligand-based emission peak at 435 nm. **1** can be stable in air and acid media, but loose crystallinity after exposure to water over 12 h and in basic media. TG and XRD study indicates that **1** can be stable up to 200 °C.

We summarized the hydrothermal stability data of Zr-MOFs, calculated the NBO (nature bond orbital) charges of the coordinating oxygen atoms of the corresponding carboxylate ligands and analyzed the influencing factors. We demonstrated that NBO charges of coordinating atoms of the ligands can be used to explain the hydrothermal stability of Zr-MOFs. The higher NBO charges of the coordinated oxygen atoms of the carboxylate linkers, the stronger Zr-O, which results in higher hydrothermal stabilities. The high NBO charge on OH^- explained why Zr-MOFs are usually unstable in basic media. In acidic solution, H_3O^+ cannot attack Zr-O bonds effectively and also suppress the concentration of OH^- in water. Therefore, Zr-MOFs are usually stable in acidic media. But in concentrated acid, the Zr-O could be protonated, leading to the weakening of the Zr-O bond. Some Zr-MOFs were reported having relatively poor hydrothermal stability. Based on the NBO calculations, we think the main reason is due to the capillary forces, which could be eliminated by choosing proper activation processes. These Zr-MOFs might be found to be stable if exchanged with

acetone or dichloromethane before activation process. The NBO calculation and the stability data in Table 1 suggest that Zr-MOFs should be stable in water (> 12 h) if the NBO charge of the O of the carboxylate ligands is greater than -0.756. Besides the known influencing factors, the summarized data also suggest the water stability of Zr-MOFs increases in the following order: 6-connected Zr_6 core > 8-connected Zr_6 core > 10-connected Zr_6 core > 12-connected Zr_6 core. The significance of this factor needs to be further investigated.

Our future study will focus on the design and synthesis of new porous Zr- MOFs with high hydrothermal stability.

Dalton Transactions RSCPublishing

PAPER

	Sample	Linker	NBO of the linker[a]	Structure (connectivity of the Zr_6 core formula of the SBUs)	Pore volume (V: cm^3/g) BET (B) and Langmuir (L) surface area (m^2/g)	Thermal stability (°C)	Chemical stability	Ref
1	Zr-fum	L1	-0.815	12-connected $Zr_6O_4(OH)_4(COO)_{12}$	B: 856	260 (TG)	water for 1 week	54
2	UiO-66	L2	-0.798	12-connected $Zr_6O_4(OH)_4(COO)_{12}$	L:1300	430 (TG)	water for 2 h 1.0 M HCl for 2 h 1.0 M NaOH < 2 h, more stable than UiO-66-NH_2.	47
				12-connected $Zr_6O_4(OH)_4(COO)_{12}$	V:0.38 L:1086	430 (TG)	water for 12 h 1.0 M HCl for 12 h	37
				12-connected $Zr_6O_4(OH)_4(COO)_{12}$ 12-connected $Zr_6O_4(OH)_4(COO)_{12}$	B: 1080	450 (TG) 350 for 2h (XRD)	water for 24 h 1.0 M HCl for 24 h water for 24h	32
					B: 700 (no modulator); 600 (30 equiv benzoic acid); 1400 (30 equiv acetic acid)	<300 (30equiv benzoic acid) （XRD） >300 (no and 30equiv acetic acid) (XRD)		52
3	MIL-140A	L2	-0.798	Zr oxide chain ZrO(BDC)[g]	V: 0.18 B: 415	450 (VTXRD)	boiling water for 15 h	14
4	UiO-66-NH_2	L3	-0.796 -0.790	12-connected $Zr_6O_4(OH)_4(COO)_{12}$	L: 1250	290 (VTXRD)	water for 12 h 1.0 M HCl for 12 h	47
					B: 1005	350 for 2h (XRD)		32
5	UiO-66-F	L4	-0.774/-0.794 -0.793/-0.794	12-connected $Zr_6O_4(OH)_4(COO)_{12}$	V: 0.26 B: 919	360 (TG)	unstable in water, acetic acid, 1.0 M HCl, more stable than No. 15 (SI of Ref 37).	37
9	UiO-66-CF_3	L5	-0.770/-0.784 -0.793	12-connected $Zr_6O_4(OH)_4(COO)_{12}$	V: 0.27 L: 739	350 (TG)	water for 12 h 1.0 M HCl for 12 h	37

6	UiO-66-Cl	L6	-0.768/-0.779 -0.793/-0.795	12-connected $Zr_6O_4(OH)_4(COO)_{12}$	V: 0.23 B: 430	420 (TG)	-	55
7	UiO-66-Br	L7	-0.769 -0.793	12-connected $Zr_6O_4(OH)_4(COO)_{12}$	L: 899	480 (TG) 450 (VTXRD)	water for 2 h 1.0 M HCl for 2 h 1.0 M NaOH < 2 h, >No. 13, < UiO-66-NO_2	47
8	UiO-66-I	L8	-	12-connected $Zr_6O_4(OH)_4(COO)_{12}$	V: 0.27 L: 799	360 (TG) 450 (VTXRD)	water for 12 h 1.0 M HCl for 12 h	38
10	UiO-66-CO_2H	L9	-0.763/-0.783 -0.792/-0.791	12-connected $Zr_6O_4(OH)_4(COO)_{12}$	0. 28 L: 842	340 (TG) 360 (VTXRD)	water for 12 h 1.0 M HCl for 12 h	38
11	UiO-66-NO_2	L10	-0.766/-0.778 -0.786/-0.792	12-connected $Zr_6O_4(OH)_4(COO)_{12}$	L: 856	310 (VTXRD)	water for 2 h 1.0 M HCl for 2 h 1.0 M NaOH < 2 h, more stable than UiO-66	47
12	UiO-66-SO_3H	L11	-0.741/-0.779 -0.785/-0.789	12-connected $Zr_6O_4(OH)_4(COO)_{12}$	V: 0.26 L: 842	260 (TG) 220 (VTXRD)	water for 12 h 1.0 M HCl for 12 h	38
14	UiO-66-$(CH_3)_2$	L12	-0.799/-0.794	12-connected $Zr_6O_4(OH)_4(COO)_{12}$	B: 868 L: 968	490 (TG)	in air for 30 days in water for 10 days pH=14 for 2 h pH=1 for 2 h	56
13	UiO-66-$(OH)_2$	L13	-0.805/-0.770	12-connected $Zr_6O_4(OH)_4(COO)_{12}$	V:0.30 B: 755	240 (TG)	-	55
15	UiO-66-F_2	L14	-0.770/-0.793	12-connected $Zr_6O_4(OH)_4(COO)_{12}$	V: 0.28 L: 836	350 (TG)	unstable in water , acetic acid, 1.0 M HCl (<12 h)	37
16	UiO-66-Cl_2	L15	-0.763/-0.779	12-connected $Zr_6O_4(OH)_4(COO)_{12}$	V: 0.21 L: 609	390 (TG)	water for 12 h 1.0 M HCl for 12 h	37
17	UiO-66-Br_2	L16	-0.761/-0.786	12-connected $Zr_6O_4(OH)_4(COO)_{12}$	V: 0.12 L: 339	390 (TG)	water for 12 h 1.0 M HCl for 12 h	37
18	UiO-66-$(CF_3)_2$	L17	-0.765/-0.777	12-connected $Zr_6O_4(OH)_4(COO)_{12}$	V: 0.24 L: 503	340 (TG)	-	55
19	UiO-66-$(CO_2H)_2$	L18	-0.759/-0.773	12-connected $Zr_6O_4(OH)_4(COO)_{12}$	V: 0.08 L: 217	290 (TG)	water for 12 h 1.0 M HCl for 12 h	37
20	DUT-67	L19	-0.786/-0.798	8-connected $Zr_6O_6(OH)_2(COO)_8(Ac)_2$	V: 0.44 B: 1064	300 (TG) (no obvious platform)	HCl (conc.) for 3d water for 24 h	57
21	DUT-68	L19	-0.786/-0.798	binodal 8-connected $Zr_6O_6(OH)_2(COO)_9(Ac)$	V: 0.41 B: 891	300 (TG) (no obvious platform)	HCl (conc.) for 3d water for 24 h	57
22	DUT-69	L19	-0.786/-0.798	10-connected $Zr_6O_4(OH)_4(COO)_{10}(Ac)_2$	V:0.31 B: 560	300 (TG) (no obvious platform)	HCl (1 M) for 1d, decomposes in strong acidic media water for 1d	57
37	DUT-51	L20	-0.690/-0.697	8-connected $Zr_6O_6(OH)_2(COO)_8(BC^f)_2(DMF)_6$	V:1.08 B: 2325	150 (TG)	water for 12 h	58
23	Zr-2,6-NDC	L21	-0.790	12-connected $Zr_6O_4(OH)_4(COO)_{12}$	V: 0.54 B: 1287	400 (VTXRD)	unstable in water (<15 h)	14
24	MIL-140B	L21	-0.790	Zr oxide chain $ZrO(NDC)^g$	V: 0.18 B: 460	400 (VTXRD)	boiling water for 15 h	14

25	Zr-1,4-NDC	L22	-0.787/-0.790	12-connected $Zr_6O_4(OH)_4(COO)_{12}$	B:615 L:712	400 (TG)	-	59
26	UiO-67	L23	-0.788	12-connected $Zr_6O_4(OH)_4(COO)_{12}$	B:2145	450 (TG) 350 < 2h (XRD)	unstable in water, 0.1 M HCl, (<24 h)	32
					B: 270 (no modulator); 2400 (30 equiv acetic acid); 3000 (30 equiv benzoic acid)	490 (TG) >300 (XRD)	unstable in water (<24 h)	52
					-	-	stable in water, collapse during activation from H_2O	33
27	MIL-140C	L23	-0.788	Zr oxide chain $ZrO(BPDC)^g$	V: 0.27 B: 670	500 (VTXRD)	boiling water for 15 h	14
28	UiO-BIPY	L24	-0.776/-0.788	12-connected $Zr_6O_4(OH)_4(COO)_{12}$	B: 2385	480 (TG) 350 for 2h (XRD)	unstable in water, 0.1 M HCl (<24 h)	32
29	Zr–AzoBDC	L25	-0.781/-0.779	12-connected $Zr_6O_4(OH)_4(COO)_{12}$	3000 (Sox)	400 (TG) As[b]: 280, Sox[b]:400 (VTXRD)	stable in air and moisture unstable in water (<24 h)	51
30	Zr–Cl_2AzoBDC	L26	-0.744	12-connected $Zr_6O_4(OH)_4(COO)_{12}$	V: 0.94 B: 2226	400 (VTXRD)	unstable in water (<24 h)	60
31	MIL-140D	L26	-0.744	Zr oxide chain $ZrO(Cl_2AzoBDC)^g$	V: 0.29 B: 701	400 (VTXRD)	boiling water for 15 h, showing some decomposition	14
32	TPDC-2CH_3 (PCN-56)	L27	-0.781	12-connected $Zr_6O_4(OH)_4(COO)_{12}$	B: 3741	400 (TG)	pH=2 for 2 d pH=11 for 1 d	12
33	TPDC-4CH_3 (PCN-57)	L28	-0.780	12-connected $Zr_6O_4(OH)_4(COO)_{12}$	B: 2572	370 (TG)	pH=11 for 2 d pH=2 for 7 d	12
34	TPDC-2CH_2N_3 (PCN-58)	L29	-0.756/-0.758	12-connected $Zr_6O_4(OH)_4(COO)_{12}$	B: 2185	260 (TG)	pH=2 for 20 h H_2O for 24 h pH=11 for 1 d	12
35	TPDC-4CH_2N_3 (PCN-59)	L30	-	12-connected $Zr_6O_4(OH)_4(COO)_{12}$	BET:1279	260 (TG)	pH=2 for 20 h H_2O for 72 h pH=11 for 24 h	12
36	PIZOF-OMe	L31	-0.775/-0.774	12-connected interpenetrated $Zr_6O_4(OH)_4(COO)_{12}$	V: 0.68 B: 1250 (Ar)	325 for 1 h （XRD）	atmospheric moisture (no XRD)	61
38	Zr-BTC-acetic	L32	-0.813	6-connected $Zr_6O_4(OH)_4(COO)_6(Ac)_6$	V: 0.78 B:1606; L:1864	270 (VTXRD)	HCl (conc.) ，boiling water , pH=10 for 24 h	43
39	Zr-BTC-formic (MOF-808)	L32	-0.813	6-connected $Zr_6O_4(OH)_4(COO)_6$(formate)$_6$	V: 0.90 B: 2330; L: 2770	230 (VTXRD) ≤140 (Vacuum for 12h) (XRD)	HCl (conc.)，boiling water, pH=10 for 24 h	43
					V: 0.84 B: 2060L: 2390		Reduced BET after water adsorption and desorption.	16
40	Zr-BTC-propionate	L32	-0.813	6-connected $Zr_6O_4(OH)_4(COO)_6$(propionate)$_6$	V: 0.75 B: 1408; L: 1633	250 (VTXRD)	HCl (conc.)，boiling water , pH=10 for 24 h	43

41	Zr-BTB	L33	-0.788	6-connected interpenetrate 2D->3D $Zr_6O_4(OH)_4(COO)_6(OH)_2(H_2O)_2$	V: 0.27 BET: 613	280 (TG)	low stability (no XRD)	62
42	MOF-841	L34	-0.790	8-connected $Zr_6O_4(OH)_4(COO)_8(HCOO)_4(H_2O)_4$	B: 1390 L: 1540 V: 0.53	380 (TG)	stable in water (no XRD)	16
43	Zr-TCPS	L35	-0.790	8-connected $Zr_6O_4(OH)_4(COO)_8(OH)_4(H_2O)_4$	B: 1039 L: 1512 V: 0.56	>200 for 12h <250 for 3h（XRD）	air for 14 d pH=0-5 for 24 h water for 12 h	this work
44	PCN-521	L36	-0.785	8-connected $Zr_6(OH)_8(COO)_8(OH)_8$	BET: 3411	450 (TG)	air for 24 h	17
45	PCN-221	L37	-0.784[d]	12-connected[e] $[Zr_8O_6(COO)_{12}]^{8+}$	V:0.76(no M) B: 1936 (no M) L: 2660 (no M)	fresh[c] : 320 (no M), 320 (Fe), 380(Co) Activated [c] : 360 (no M) 330 (Fe), 350 (Co) (TG)		63
46	PCN-222	L37	-0.784 [d]	8-connected $Zr_6(OH)_8(COO)_8(OH)_8$	V: 1.31(no M), 1.56 (Fe), 1.65 (Ni), 1.31(Co) B:2223(no M),2200 (Fe), 2283 (Ni), 1864 (Co)	fresh: 380 (no M) 410 (Ni), 330 (Fe) 310 (Co) activated: 350(no M) 380 (Ni), 350 (Fe) 330 (Co) (TG)	HCl (conc.), water for 24 h	15
47	PCN-224	L37	-0.784 [d]	6-connected $Zr_6(OH)_8(COO)_6(OH)_{10}(H_2O)_2$	V: 1.59 B: 2600 (Ni)	fresh: 350 activated : 350(no M) 400(Ni) 330(Co) (TG)	pH=0-11 for 24 h	13
48	PCN-225	L37	-0.784 [d]	8-connected $Zr_6O_4(OH)_4(COO)_8(OH)_4(H_2O)_4$	B: 1902 (no M) 2080 (Zn)	470 (TG)	pH=1-11for12 h	35
49	MOF-525	L37	-0.784 [d]	12- connected $Zr_6O_4(OH)_4(COO)_{12}$	B:2620	-	water, H_2O/acetic acid (50/50, vol) for 24 h	64
50	MOF-545	L37	-0.784 [d]	8-connected $Zr_6O_8(COO)_8(H_2O)_8$	B:2260	-	-	64
51	H_2O		-0.997					
52	OH^-		-1.403					

a. When the NBO charges of O atoms are different, the NBO charges of the O atoms of the COO^- group which is next to the substitute group are given in the first line (The NBO charge of the O on the same side of the substitute is given first; if NBO charges of both Os are the same, only one number are given); the NBO charges of the rest O atoms are given in the second line.
b. "As" represents as-synthesized sample, "Sox "represents Soxhlet-extraction sample
c. "fresh" represents fresh sample, "activated "represents activated sample
d. The NBO charge of L37 (no M).
e. The SBU has a Zr_8 core instead of the common Zr_6 core.
f. BC = benzoate
g. The formula of the Zr-MOF.

Scheme 1 The carboxylate ligands

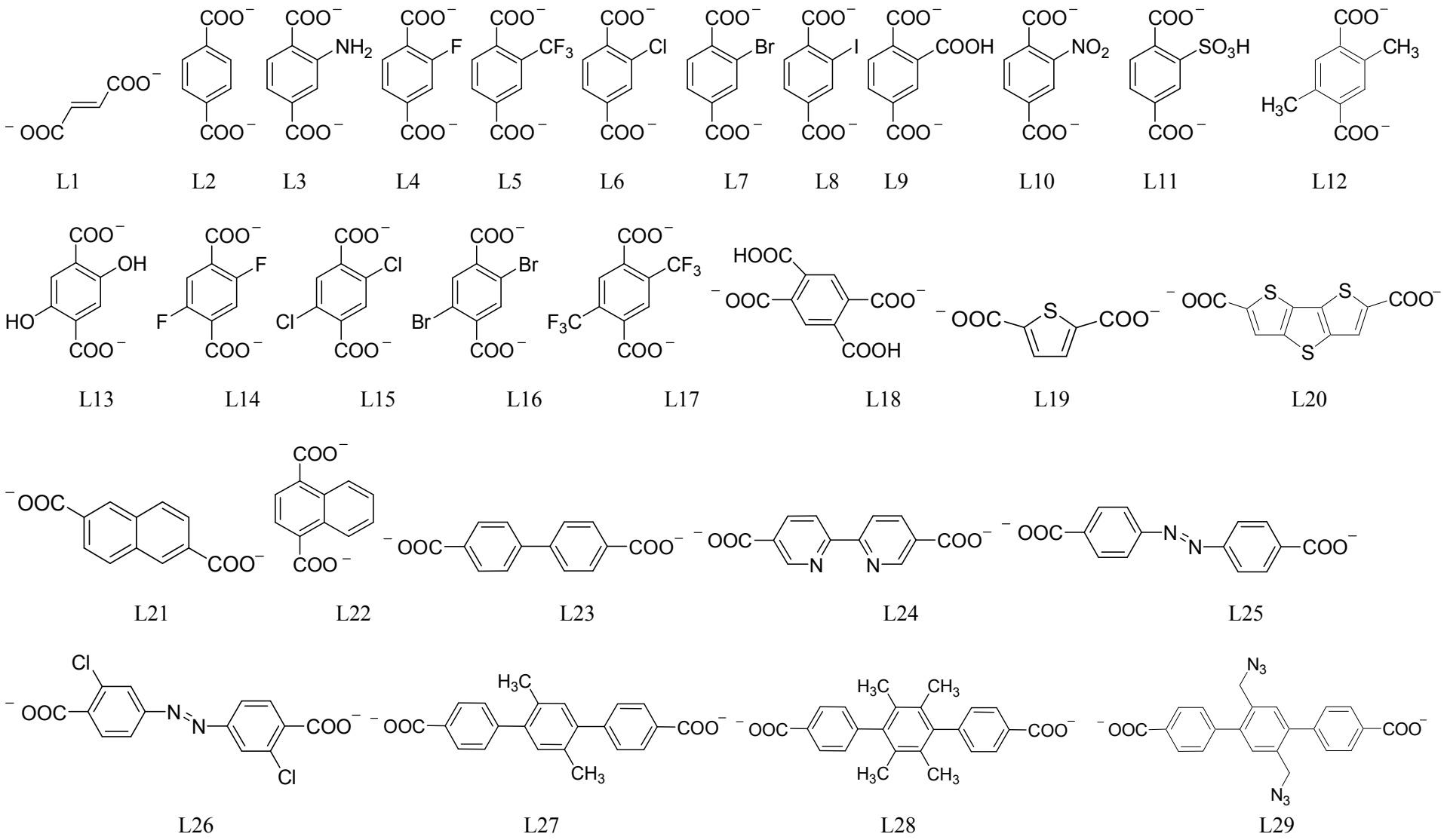

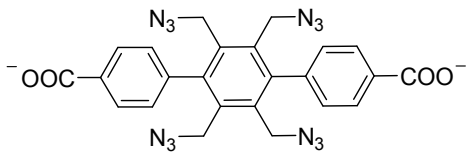

L30

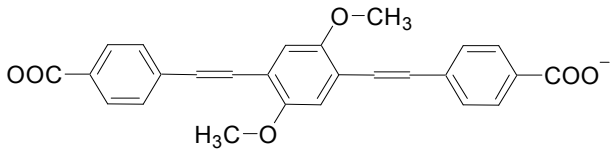

L31

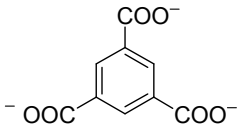

L32

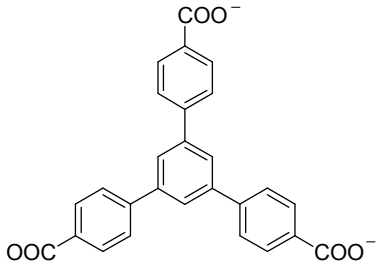

L33

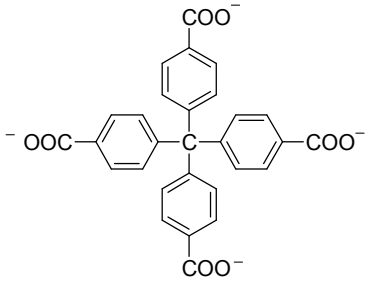

L34

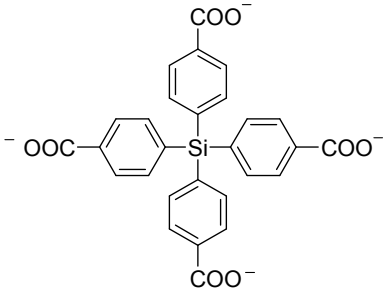

L35

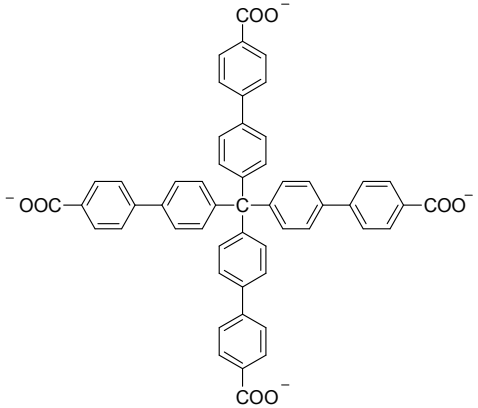

L36

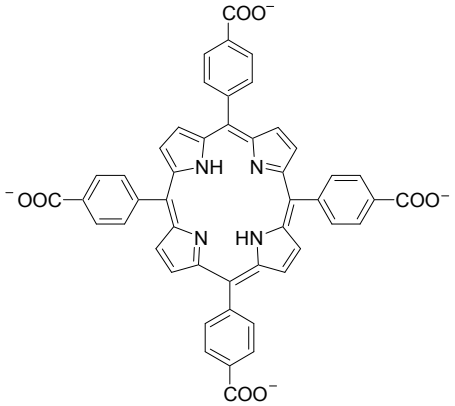

L37 (no M)

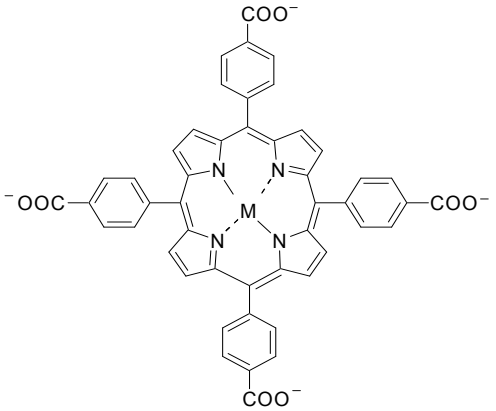

L37 (M=Fe, Co, Ni, Zn)

Dalton Transactions

RSCPublishing

PAPER

Acknowledgements

We thank National Natural Science Foundation of China (Project, 21071082,21171095), the Key International (Regional) Joint Research Program of NSF (Grant No. 2014456), the Natural Science Foundation of Education Department of Jiangsu Province (No. 13kjb150022) , and the Priority Academic Program Development of Jiangsu Higher Education Institutions (PAPD) for their support for our work.

Notes and References

[a]Department of Chemistry, School of Chemistry and Materials Science, Nanjing Normal University, Nanjing 210023, China. Email: fangmin@njnu.edu.cn, wuyong@njnu.edu.cn
[b]School of Chemistry and Bioengineering, Nanjing Normal University Taizhou College, Taizhou 225300, China
[c]Jiangsu Collaborative Innovation Center of Biomedical Functional Materials，Jiangsu Key Laboratory of Biomedical Materials，College of Chemistry and Materials Science，Nanjing Normal University，Nanjing 210046，China.
[d]College of Chemistry and Chemical Engineering, State Key Laboratory of Materials-Oriented Chemical Engineering, Nanjing Tech University, Nanjing 210009, China
[e]State Key Laboratory of Coordination Chemistry, Nanjing University, Nanjing 210093, China
[f] Jiangsu Key Laboratory for NSLSCS, Nanjing Normal University, Nanjing 210023, China
†Structures of the same topology but based on derivatives of the same ligand are counted as one structure.
Electronic supplementary information (ESI) available: details for crystallographic data, H_2 adsorption/desorption isotherms of the as-synthesized sample at 77 K

1 H Furukawa, K. E. Cordova, M. O'Keeffe and O. M. Yaghi, *Science*,2013, **341**, 974-+.
2 J. E. Mondloch, W. Bury, D. Fairen-Jimenez, S. Kwon, E. J. DeMarco, M. H. Weston, A. A. Sarjeant, S. T. Nguyen, P. C. Stair, R. Q. Snurr, O. K. Farha and J. T. Hupp, *J. Am. Chem. Soc.*, 2013, **135**, 10294-10297.
3 A. Dhakshinamoorthy, M. Opanasenko, J. Cejka an.d H. Garcia, *Catal. Sci. Technol.*, 2013, **3**, 2509-2540.
4 C. Wang, D. M. Liu and W. B. Lin, *J. Am. Chem. Soc*, 2013, **135**, 13222-13234.
5 L. E. Kreno, K. Leong, O. K. Farha, M. Allendorf, R. P. Van Duyne and J. T. Hupp, *Chem. Rev*, 2011, **112**, 1105-1125.
6 P. Sippel, D. Denysenko, A. Loidl, P. Lunkenheimer, G. Sastre and D. Volkmer, *Adv. Funct. Mater.,* 2014, **24**, 3885-3896.
7 F. Fresno, R. Portela, S. Suarez and J. M. Coronado, *J. Mater. Chem. A*, 2014, **2**, 2863-2884.
8 D. Y. Lee, D. V. Shinde, E.-K. Kim, W. Lee, I.-W. Oh, N. K. Shrestha, J. K. Lee and S.-H. Han, *Microporous Mesoporous Mater.*, 2013, **171**, 53-57.
9 J. Yang, P. X. Xiong, C. Zheng, H. Y. Qiu and M. D. Wei, *J. Mater. Chem. A*, 2014, **2**, 16640-16644.
10 H. Wu, T. Yildirim and W. Zhou, *J. Phys. Chem. Lett.*, 2013, **4**, 925-930.
11 J. H. Cavka, S. Jakobsen, U. Olsbye, N. Guillou, C. Lamberti, S. Bordiga and K. P. Lillerud, *J. Am. Chem. Soc.*, 2008, **130**, 13850-13851.
12 H.-L. Jiang, D. Feng, T.-F. Liu, J.-R. Li and H.-C. Zhou, *J. Am. Chem. Soc.*, 2012, **134**, 14690-14693.
13 D. Feng, W.-C. Chung, Z. Wei, Z.-Y. Gu, H.-L. Jiang, Y.-P. Chen, D. J. Darensbourg and H.-C. Zhou, *J. Am. Chem. Soc.*, 2013, **135**, 17105-17110.
14 V. Guillerm, F. Ragon, M. Dan-Hardi, T. Devic, M. Vishnuvarthan, B. Campo, A. Vimont, G. Clet, Q. Yang, G. Maurin, G. Férey, A. Vittadini, S. Gross and C. Serre, *Angew. Chem. Int. Ed.*, 2012, **51**, 9267-9271.
15 D. Feng, Z.-Y. Gu, J.-R. Li, H.-L. Jiang, Z. Wei and H.-C. Zhou, *Angew. Chem. Int. Ed.*, 2012, **51**, 10307-10310.
16 H. Furukawa, F. Gándara, Y.-B. Zhang, J. Jiang, W. L. Queen, M. R. Hudson and O. M. Yaghi, *J. Am. Chem. Soc.*, 2014.
17 M. Zhang, Y.-P. Chen, M. Bosch, T. Gentle, K. Wang, D. Feng, Z. U. Wang and H.-C. Zhou, *Angew. Chem. Int. Ed.*, 2014, **53**, 815-818.
18 H. Chun, D. Kim, D. N. Dybtsev and K. Kim, *Angew. Chem., Int. Ed.*, 2004, **43**, 971-974.
19 M. Dincă, A. Dailly and J. R. Long, *Chem.-Eur. J.*, 2008, **14**, 10280-10285.
20 J. M. Gotthardt, K. F. White, B. F. Abrahams, C. Ritchie and C. Boskovic, *Cryst. Growth Des.*, 2012, **12**, 4425-4430.
21 B. L. Chen, M. Eddaoudi, T. M. Reineke, J. W. Kampf, M. O'Keeffe and O. M. Yaghi, *J. Am. Chem. Soc.*, 2000, **122**, 11559-11560.
22 J. Kim, B. L. Chen, T. M. Reineke, H. L. Li, M. Eddaoudi, D. B. Moler, M. O'Keeffe and O. M. Yaghi, *J. Am. Chem. Soc.*, 2001, **123**, 8239-8247.
23 L. Wen, P. Cheng and W. Lin, *Chem. Commun.*, 2012, **48**, 2846-2848.
24 L. Wen, P. Cheng and W. Lin, *Chem. Sci.*, 2012, **3**, 2288-2292.
25 D. Liu, H. Wu, S. Wang, Z. Xie, J. Li and W. Lin, *Chem. Sci.*, 2012, **3**, 3032-3037.
26 C. Tan, S. Yang, N. R. Champness, X. Lin, A. J. Blake, W. Lewis and M. Schroder, *Chem. Commun.*, 2011, **47**, 4487-4489.
27 Y. E. Cheon and M. P. Suh, *Chem. Commun.*, 2009, 2296-2298.
28 J. M. Taylor, A. H. Mahmoudkhani and G. K. H. Shimizu, *Angew. Chem.*, 2007, **119**, 809-812.
29 L. Ma, A. Jin, Z. Xie and W. Lin, *Angew. Chem. Int. Ed.*, 2009, **121**, 10089-10092.
30 W. Lu, Z. Wei, Z.-Y. Gu, T.-F. Liu, J. Park, J. Park, J. Tian, M. Zhang, Q. Zhang, T. Gentle Iii, M. Bosch and H.-C. Zhou, *Chem. Soc. Rev.*, 2014, **43**, 5561-5593.
31 R. P. Davies, R. Less, P. D. Lickiss, K. Robertson and A. J. P. White, *Cryst. Growth Des.*, 2010, **10**, 4571-4581.
32 J. B. DeCoste, G. W. Peterson, H. Jasuja, T. G. Glover, Y.-g. Huang and K. S. Walton, *J. Mater. Chem. A*, 2013, **1**, 5642-5650.
33 J. E. Mondloch, M. J. Katz, N. Planas, D. Semrouni, L. Gagliardi, J. T. Hupp and O. K. Farha, *Chem. Commun.*, 2014, **50**, 8944-8946.
34 B. Zhang and Z. Wang, *Chem. Mater.*, 2010, **22**, 2780-2789.

35 H.-L. Jiang, D. Feng, K. Wang, Z.-Y. Gu, Z. Wei, Y.-P. Chen and H.-C. Zhou, *J. Am. Chem. Soc.*, 2013, **135**, 13934-13938.
36 S. Chavan, J. G. Vitillo, D. Gianolio, O. Zavorotynska, B. Civalleri, S. Jakobsen, M. H. Nilsen, L. Valenzano, C. Lamberti, K. P. Lillerud and S. Bordiga, *Phys. Chem. Chem.Phys.*, 2012, **14**, 1614-1626.
37 S. Biswas and P. Van der Voort, *Eur. J. Inorg. Chem.*, 2013, 2154-2160.
38 S. Biswas, J. Zhang, Z. Li, Y.-Y. Liu, M. Grzywa, L. Sun, D. Volkmer and P. Van Der Voort, *Dalton Trans.*, 2013, **42**, 4730-4737
39 L. Li, S. Tang, C. Wang, X. Lv, M. Jiang, H. Wu and X. Zhao, *Chem. Commun.*, 2014, **50**, 2304-2307.
40 J. Liu, P. K. Thallapally, B. P. McGrail, D. R. Brown and J. Liu, *Chem. Soc. Rev.*, 2012, **41**, 2308-2322.
41 Y. B. He, W. Zhou, G. D. Qian and B. L. Chen, *Chem. Soc. Rev.*, 2014, **43**, 5657-5678.
42 C. Wang, O. Volotskova, K. Lu, M. Ahmad, C. Sun, L. Xing and W. Lin, *J. Am. Chem. Soc.*, 2014, **136**, 6171-6174.
43 W. Liang, H. Chevreau, F. Ragon, P. D. Southon, V. K. Peterson and D. M. D'Alessandro, *CrystEngComm*, 2014, **16**, 6530-6533.
44 L. Liu, J. Ding, M. Li, X. Lv, J. Wu, H. Hou and Y. Fan, *Dalton Trans.*, 2014, **43**, 12790-12799.
45 L. Valenzano, B. Civalleri, S. Chavan, S. Bordiga, M. H. Nilsen, S. Jakobsen, K. P. Lillerud and C. Lamberti, *Chem. Mater.*, 2011, **23**, 1700-1718.
46 P. Lu, Y. Wu, H. Kang, H. Wei, H. Liu and M. Fang, *J. Mater. Chem. A*, 2014, **2**, 16250-16267.
47 M. Kandiah, M. H. Nilsen, S. Usseglio, S. Jakobsen, U. Olsbye, M. Tilset, C. Larabi, E. A. Quadrelli, F. Bonino and K. P. Lillerud, *Chem. Mater.*, 2010, **22**, 6632-6640.
48 H. Li, M. Eddaoudi, M. O'Keeffe and O. M. Yaghi, *Nature*, 1999, **402**, 276-279.
49 A. P. Nelson, O. K. Farha, K. L. Mulfort and J. T. Hupp, *J. Am. Chem. Soc.*, 2009, **131**, 458-+.
50 L. Ma, A. Jin, Z. Xie and W. Lin, *Angew. Chem., Int. Ed.*, 2009, **48**, 9905-9908.
51 A. Schaate, S. Dühnen, G. Platz, S. Lilienthal, A. M. Schneider and P. Behrens, *Eur. J. Inorg. Chem.*, 2012, **2012**, 790-796.
52 A. Schaate, P. Roy, A. Godt, J. Lippke, F. Waltz, M. Wiebcke and P. Behrens, *Chem.–Eur. J.*, 2011, **17**, 6643-6651.
53 P. Kuesgens, M. Rose, I. Senkovska, H. Froede, A. Henschel, S. Siegle and S. Kaskel, *Microporous Mesoporous Mater.*, 2009, **120**, 325-330.
54 G. Wißmann, A. Schaate, S. Lilienthal, I. Bremer, A. M. Schneider and P. Behrens, *Microporous Mesoporous Mater.*, 2012, **152**, 64-70.
55 D. Cunha, C. Gaudin, I. Colinet, P. Horcajada, G. Maurin and C. Serre, *J. Mater. Chem. B*, 2013, **1**, 1101-1108.
56 Y. Huang, W. Qin, Z. Li and Y. Li, *Dalton Trans.*, 2012, **41**, 9283-9285.
57 V. Bon, I. Senkovska, I. A. Baburin and S. Kaskel, *Cryst. Growth Des.*, 2013, **13**, 1231-1237.
58 V. Bon, V. Senkovskyy, I. Senkovska and S. Kaskel, *Chem. Commun.*, 2012, **48**, 8407-8409.
59 S. J. Garibay and S. M. Cohen, *Chem. Commun.*, 2010, **46**, 7700-7702.
60 Q. Yang, V. Guillerm, F. Ragon, A. D. Wiersum, P. L. Llewellyn, C. Zhong, T. Devic, C. Serre and G. Maurin, *Chem. Commun.*, 2012, **48**, 9831-9833.
61 R. Wang, Z. Wang, Y. Xu, F. Dai, L. Zhang and D. Sun, *Inorg. Chem.*, 2014, **53**, 7086-7088.
62 A. Schaate, P. Roy, T. Preusse, S. J. Lohmeier, A. Godt and P. Behrens, *Chem.-Eur. J.,* 2011, **17**, 9320-9325.
63 D. Feng, H.-L. Jiang, Y.-P. Chen, Z.-Y. Gu, Z. Wei and H.-C. Zhou, *Inorg. Chem.*, 2013, **52**, 12661-12667.
64 W. Morris, B. Volosskiy, S. Demir, F. Gándara, P. L. McGrier, H. Furukawa, D. Cascio, J. F. Stoddart and O. M. Yaghi, *Inorg. Chem.*, 2012, **51**, 6443-6445.

Content

A new Zr-MOF based on tetrakis(4-carboxyphenyl) silane was synthesized, and factors affecting the hydrothermal stability of Zr-MOFs were discussed.